Acta Biomaterialia 41 (2016) 193–203

Contents lists available at ScienceDirect

Acta Biomaterialia

journal homepage: www.elsevier.com/locate/actabiomat

Full length article

Structural determinants of hydration, mechanics and fluid flow in freeze-dried collagen scaffolds

G.S. Offeddu [a,b,1], J.C. Ashworth [b,1], R.E. Cameron [b], M.L. Oyen [a,*]

[a] Nanoscience Centre, Department of Engineering, University of Cambridge, Cambridge CB3 0FF, UK
[b] Cambridge Centre for Medical Materials, Department of Materials Science and Metallurgy, University of Cambridge, Cambridge CB3 0FF, UK

ARTICLE INFO

Article history:
Received 2 February 2016
Received in revised form 18 April 2016
Accepted 13 May 2016
Available online 30 May 2016

Keywords:
Collagen scaffolds
Micro-CT
Scaffold swelling
Indentation
Poroelasticity

ABSTRACT

Freeze-dried scaffolds provide regeneration templates for a wide range of tissues, due to their flexibility in physical and biological properties. Control of structure is crucial for tuning such properties, and therefore scaffold functionality. However, the common approach of modeling these scaffolds as open-cell foams does not fully account for their structural complexity. Here, the validity of the open-cell model is examined across a range of physical characteristics, rigorously linking morphology to hydration and mechanical properties. Collagen scaffolds with systematic changes in relative density were characterized using Scanning Electron Microscopy, X-ray Micro-Computed Tomography and spherical indentation analyzed in a time-dependent poroelastic framework. Morphologically, all scaffolds were mid-way between the open- and closed-cell models, approaching the closed-cell model as relative density increased. Although pore size remained constant, transport pathway diameter decreased. Larger collagen fractions also produced greater volume swelling on hydration, although the change in pore diameter was constant, and relatively small at ~6%. Mechanically, the dry and hydrated scaffold moduli varied quadratically with relative density, as expected of open-cell materials. However, the increasing pore wall closure was found to determine the time-dependent nature of the hydrated scaffold response, with a decrease in permeability producing increasingly elastic rather than viscoelastic behavior. These results demonstrate that characterizing the deviation from the open-cell model is vital to gain a full understanding of scaffold biophysical properties, and provide a template for structural studies of other freeze-dried biomaterials.

Statement of Significance

Freeze-dried collagen sponges are three-dimensional microporous scaffolds that have been used for a number of exploratory tissue engineering applications. The characterization of the structure-properties relationships of these scaffolds is necessary to understand their biophysical behavior in vivo. In this work, the relationship between morphology and physical properties in the dry and hydrated states was investigated across a range of solid concentrations in the scaffolds. The quantitative results provided can aid the design of scaffolds with a target trade-off between mechanical properties and structural features important for their biological activity.

1. Introduction

The fast-growing field of tissue engineering produces new developments every day [1], yet applications outside the laboratory are still often limited to the repair of planar tissues or organs that do not act predominantly as load-bearing structures [2]. Repair of large tissue damage, and eventually whole organs, requires three-dimensional scaffolds with the ability to determine the fate of the cells seeded within their structure. This can only be achieved through precise understanding and control of the scaffold's structure and physical responses, as well as its interaction with cells and biomolecules [3,4].

Collagen-based scaffolds have been the platform for a number of exploratory clinical trials that showed the true potential of tissue engineering for repairing significant tissue damage [5,6]. Making up almost a third of total body protein [7], collagen provides cells with a large number of natural cues for cell attachment [8]. By means of a freeze-drying process, collagen can be formed into

* Corresponding author.
E-mail address: mlo29@cam.ac.uk (M.L. Oyen).
[1] These authors contributed equally to this work.

http://dx.doi.org/10.1016/j.actbio.2016.05.024
1742-7061/

a highly porous structure, with the pore space defined by the growth of ice crystals [9]. Recent innovations in the understanding of this process now allow pore size and anisotropy to be precisely controlled, in structures with porosity in excess of 99% [10–12]. The resulting versatility of the freeze-drying process has prompted further studies, in which microporous tissue engineering scaffolds were fabricated from a number of different polymers. These included gelatin [13] and its blend with hydroxyapatite [14], polylactic acid (PLA) [15], polycaprolactone (PCL) [16], and chitosan and alginate [17]. Methods for the characterization of key features of such microporous scaffolds, like the presence and characteristic size of transport pathways and the multi-scale mechanical response, have been developed [18,19]. Nevertheless, the relationships between solid arrangement and scaffold physical properties are still not well understood. In this study, a combination of morphological and physical characterization techniques is used to probe these relationships, focussing specifically on the response of freeze-dried collagen scaffolds according to their solid concentration. The structure of freeze-dried materials has often been approached using geometrical considerations, since their pore morphology has been observed to be similar to that of tetrakaidecahedra, showing an average of 14 faces per pore and nearly-tetrahedral vertices [20]. Equally, the materials have previously been reported to behave mechanically as open-cell foams, where the pore volume is delimited by struts only and no pore walls are present [21]. However, this model does not reflect the morphological properties of the scaffold, since pore walls have been clearly observed in multiple studies on these materials [19,22]. The potential implications of this clear deviation from the open-cell model have not yet been studied, but are likely to influence the mechanical behavior and transport characteristics of these materials, as well as affecting the surface area available for cell adhesion.

In a preliminary study by the authors, it was shown that while the mechanical response of these scaffolds varies with solid concentration at the macroscale, it remains constant at the scale of a single cell [19]. As the material making up the structure remains unchanged and is not otherwise densified with increasing concentration, it must therefore occupy more volume in the form of either thicker struts or an increasing number of walls per pore. The aim of the current study is therefore to use rigorous morphological characterization methods to understand these changes in more detail, and to correlate them with the observed physical properties of each scaffold. The morphology is first investigated in the dry state, for ease of characterization by Scanning Electron Microscopy (SEM) and X-ray Micro-Computed Tomography (Micro-CT). As the materials are designed to function in the highly hydrated environment of the body, particular attention is then given to the effect of hydration on both morphology and mechanical properties. This includes the movement of fluid through the structure and its effect on the time-dependent deformation of the materials. In this way, the relevance of the open-cell model is assessed for predicting and explaining the functional properties required of a freeze-dried tissue engineering scaffold.

2. Experimental methods

2.1. Scaffold fabrication

Insoluble fibrillar type I collagen from bovine Achilles tendon (Sigma-Aldrich, UK) was used for scaffold fabrication using a freeze-drying technique, as previously described [19]. Briefly, collagen was suspended in 0.05 M acetic acid (Alfa-Aesar, UK), at a concentration controlled between 0.5% w/V and 1.5% w/V in increments of 0.25% w/V, and blended to form a homogeneous slurry. Freeze-drying of the slurry took place in silicone molds at approximately 5 mm filling height. The freezing step was carried out at −20 °C, following a cooling rate of 0.5 °C/min from room temperature, and the drying step took place at 0°C under a vacuum of 80 mTorr. The scaffolds were then cross-linked with 1-ethyl-3-(3-dimethylaminopropyl) carbodiimide hydrochloride (EDC, Sigma-Aldrich) and N-hydroxysuccinimide (NHS, Sigma-Aldrich) in ethanol-water (95% V/V), in the molar ratio 5:2:1 relative to the collagen carboxylic acid groups (EDC:NHS:COOH). The dry scaffold density, ρ^*, was measured as the weight of the samples over their volume and used in conjunction with that of collagen (ρ_S = 1.3 g/cm^3 [21]) to calculate their relative density $\left(\frac{\rho^*}{\rho_S}\right)$. The observed relationships between scaffold properties and slurry concentration are described in terms of this relative density. However, since relative density was calculated to change upon hydration (see Section 2.3), comparisons between the dry and hydrated states are described in terms of slurry concentration itself.

2.2. Morphological characterization

The morphology of the freeze-dried scaffolds was investigated by SEM in the dry state and Micro-CT in the dry and hydrated states. SEM micrographs, acquired with an EVO LS15 machine (Carl Zeiss, Germany) at an acceleration voltage of 8 kV, were used to measure the thickness of the pore walls, t_w, and struts, t_s, as a function of solid concentration in the scaffolds (Fig. 1). The expected strut diameter, $t_{s,open}$, for a tetrakaidecahedral open-cell scaffold was also calculated as a function of scaffold relative density and pore size, D_p [23]:

$$t_{s,open} = 2\sqrt{\frac{\frac{\rho^*}{\rho_S}}{1.06}}\frac{D_p}{2.78} \quad (1)$$

Measurements of D_p were made from 3D Micro-CT visualization. Samples were scanned using a Skyscan 1172 system (Bruker, BE) at 25 kV and 137 μA, with a pixel size of 4 μm. Exposure time was set at 750 ms, averaged over 2 frames, with a rotation step of 0.2°. Pore size D_p was also measured for the hydrated state, by staining samples approximately 10 mm × 10 mm × 2 mm for 48 h in a solution of 0.3% phosphotungstic acid (Sigma-Aldrich, UK) in 70% ethanol. Submerged samples were degassed under vacuum to ensure complete penetration of the staining solution. Stained samples were washed in 70% ethanol and in deionized water, before scanning in fresh deionized water at 40 kV and 250 μA with a 0.5 mm Al filter. Exposure time was increased to 1500 ms, with all other scan settings kept constant. The shadow projection images were reconstructed into 3D datasets using the Skyscan software NRecon, and binarized using the Trainable Segmentation plugin in the ImageJ software distribution FIJI. Image noise was removed using the FIJI Despeckle function in 2D, followed by a 2 × 2 × 2 median filter in 3D. Pore size D_p was calculated from 2D slices of area 8 mm^2, sampled at 100 μm spacing in three perpendicular planes. Outliers up to 2 pixels in size were removed to allow ellipse fitting using the automated Watershed and Analyse Particles functions in the FIJI software. Pore size was defined as the diameter of the circle of equivalent area to each ellipse. The average pore size for a given Micro-CT volume was calculated as the mean value over all three planes.

Micro-CT analysis was also used for numerical analysis of the pore space transport pathways through the structure, by calculation of percolation diameter as described previously [18]. Briefly, the distance accessible in a specified direction, L, to a spherical object of diameter d may be described using the following relationship:

$$L \propto (d - d_c)^{-0.88} \quad (2)$$

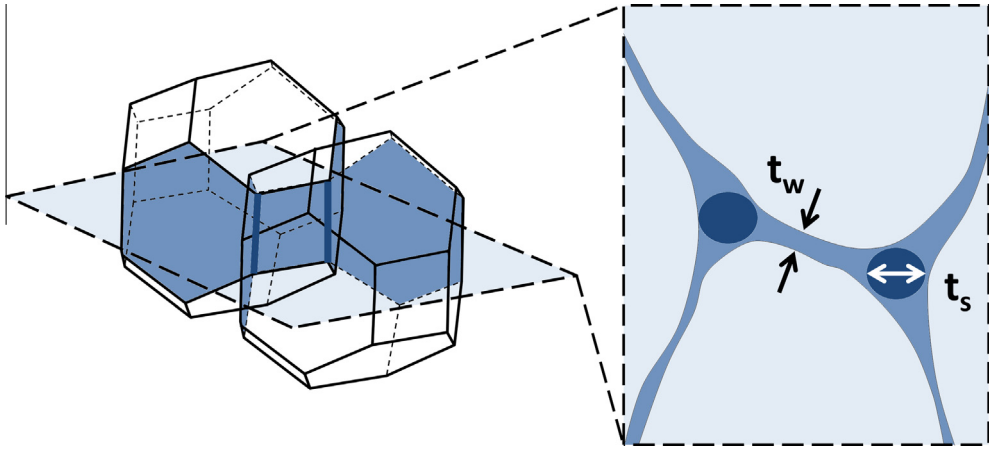

Fig. 1. Measurement of morphological features from SEM micrographs: pore wall thickness, t_w, and strut diameter, t_s. The diagram shows how pore struts (dark) are always the intersection of three distinct pore walls in the tetrakaidecahedron model used to quantify the pore geometry.

Using this relationship, successive measurements of L and d may be extrapolated to find the percolation diameter, d_c, which represents the diameter of the object that may travel through a scaffold of infinite dimensions. This critical diameter describes the characteristic size of the pathways encountered by an invading object in a specified direction [18]. Measurements of L and d were obtained using the Skyscan software CTAn, for object travel in the scaffold z-direction (i.e. the direction of solidification). The CTAn software was also used for calculation of specific surface area (SSA), the pore wall surface area per unit scaffold volume, using the 3D Analysis function. The SSA measured for each condition was then used to calculate the pore coverage fraction, γ, from the weighted average of the predicted SSA for each of the open- and closed-cell models. Whereas the theoretical SSA for the open-cell model is defined as $SSA_{open} = \frac{10.17}{D_p} c$ [23], where c is the concentration of solid in the scaffolds, the expected SSA for a tetrakaidecahedral closed-cell structure is $SSA_{closed} = \frac{8.2}{Dp}$ [24]. The pore coverage fraction of a freeze-dried scaffold, γ , may therefore be calculated using the following expression:

$$SSA = (1-\gamma)SSA_{open} + \gamma SSA_{closed} = (1-\gamma)\frac{10.17}{D_p}\left(\frac{\rho^*}{\rho_S}\right) + \gamma\frac{8.2}{D_p} \quad (3)$$

γ can assume a value between 0 and 1, where 0 corresponds to an open-cell structure (no pore walls) and 1 to a completely closed-cell structure.

2.3. Swelling studies

Scaffold samples measuring roughly 2 cm × 2 cm × 5 mm were hydrated in distilled water for 48 h and then degassed under a vacuum of 3000 mTorr for 20 min, to ensure the removal of any remaining air bubbles within the pore structure. Swelling was measured post-degassing in terms of the mass swelling ratio, Q_m, and volume swelling ratio, Q_V, calculated as:

$$Q_m = \frac{m_h}{m_d} \quad (4)$$

$$Q_V = \frac{V_h}{V_d} \quad (5)$$

where m_d and m_h are the dry and hydrated masses of the samples, and V_d and V_h indicate the volumes of the samples before and after hydration, respectively [25]. The relative density of the hydrated scaffolds was calculated as:

$$\left(\frac{\rho^*}{\rho_S}\right)_h = \frac{\left(\frac{\rho^*}{\rho_S}\right)_d}{Q_V} \quad (6)$$

and reported in Table 1 together with the corresponding dry relative density and original composition of the slurry.

The hydrated mass is the sum of the solid dry mass, m_d, and mass of water hydrating the scaffold. The latter is present in two states, free water occupying the pore spaces and water bound to collagen. The proportion of bound water was measured by manually squeezing out the free fluid until only hydrated collagen was left, with a mass $m_d + m_b$, where m_b is the mass of bound water. These were used in conjunction with Q_V to calculate the increase in pore free space $V_{p,h}/V_{p,d}$, the nominator and denominator being the pore volume in the hydrated and dry conditions, respectively. The relationship, derived in Appendix A, is:

$$\frac{V_{p,h}}{V_{p,d}} = \frac{Q_V\frac{\rho_S}{\rho^*} - 1 - \frac{m_b}{m_c}\frac{\rho_S}{\rho_w}}{\frac{\rho_S}{\rho^*} - 1} \quad (7)$$

where ρ_w is the density of water (1 g/cm^3). All calculated morphological parameters are depicted in graphs with gray markers to distinguish them from measured variables, which are given black or white markers where plotted as a function of dry or hydrated relative density, respectively.

2.4. Mechanical testing

Spherical indentation was used to characterize the time-dependent mechanical response of the scaffolds in the dry and hydrated states. Testing was performed in displacement-control on an Instron 5544 universal testing machine (Instron, US), with a glass tip of 4 mm diameter. A ramp-hold profile was used with

Table 1
Scaffold relative density resulting from each initial slurry concentration, measured directly for the dry state, and calculated using measurements of bulk swelling (Q_V) for the hydrated state, shown as mean ± standard deviation.

Slurry concentration (% w/V)	Dry relative density, $\left(\frac{\rho^*}{\rho_S}\right)_d$	Hydrated relative density, $\left(\frac{\rho^*}{\rho_S}\right)_h$
0.5	0.0053 ± 0.0006	0.0045 ± 0.0005
0.75	0.0078 ± 0.0006	0.0062 ± 0.0005
1.0	0.0100 ± 0.0005	0.0080 ± 0.0004
1.25	0.0115 ± 0.0006	0.0090 ± 0.0005
1.5	0.0149 ± 0.0004	0.0112 ± 0.0003

a ramp of ten seconds to an indentation depth of 0.2 mm, followed by a hold of 120 s. A viscoelastic framework of analysis was used for both dry and hydrated scaffolds, while the hydrated samples (degassed) were also investigated within a poroelastic framework. Both frameworks were applied using algorithms based on exponential fitting of the load relaxation profile [26–28]. Viscoelastic analysis yields the instantaneous modulus, E_0, equilibrium modulus, E_{inf}, and viscoelastic ratio, $R = E_{inf}/E_0$, of the scaffolds. Poroelastic analysis yields the drained modulus, E_p, Poisson's ratio, ν, and hydraulic permeability, K, of the hydrated scaffolds, which dictates the mobility of water within the porous structure.

The hydraulic permeability was also measured directly using a custom-built rig that measures the pressure difference between two sides of a sample as distilled water is pressured through it by use of a syringe pump (Fig. 2). Darcy's law was applied to obtain the hydraulic permeability:

$$K = \frac{k}{\mu} = \frac{Q\Delta x}{Ap} \tag{8}$$

where k is the intrinsic permeability of the material, μ is the dynamic viscosity of water (8.90×10^{-4} Pa s) [20], Q is the volumetric flow rate, A the surface area, Δx the thickness of the sample, and p the pressure increase. Two volumetric flow rates (0.05 mL/hour and 0.1 mL/hour) were applied consecutively to each sample to check for flow-independent linearity. Since this was observed in all cases, the average hydraulic permeability over both flow rates was calculated.

2.5. Statistical analysis

All morphological analysis was averaged over at least three regions, from at least two different physical samples per condition. Likewise, all swelling and mechanical measurements were made from at least two different samples per condition. Each value is reported as mean and standard deviation of these measurements. The reported trends with scaffold relative density were tested for statistical significance using one-way analysis of variance (ANOVA). Where comparisons between two different trends are made, statistical significance was assessed using paired t-tests. A probability value of 95% ($p < 0.05$) was used to determine significance for both types of test. When comparison to a theoretical trend is made, the exponent of each trend, n, where $y = x^n$, is also reported as mean and standard deviation, with the accompanying R^2 value to indicate how well the data fits this trend. All statistical analysis was carried out using the standard statistics package in Origin Pro 2015 (Origin Lab, US).

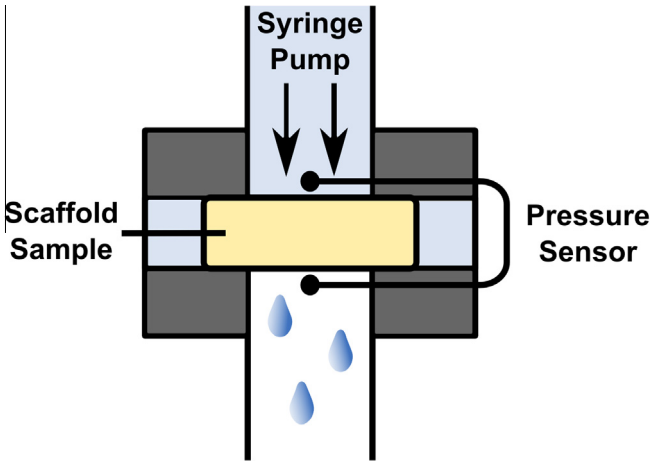

Fig. 2. Schematic of direct permeability measurement rig. As the sample was placed between the two holders, care was taken in order to avoid straining it, and therefore affecting the permeability results.

3. Results

3.1. Dry morphology

The SEM micrographs depicted in Fig. 3a–c show a qualitatively similar pore architecture for all concentrations: pore spaces are defined by walls that partially enclose an empty volume. Some slight pore size variation could be seen between sections, as can be expected from the stochastic nature of the ice crystallization process [29], but no systematic change was apparent with concentration.

However, a systematic increase in both pore wall and strut thicknesses could be seen with increasing concentration, as can be seen visually in Fig. 3d–f, and reported quantitatively in Fig. 4. As scaffold relative density increased, a statistically significant trend in the thicknesses of the pore walls and of the pore struts was observed ($p < 0.05$). The relative thickness of the features, t_w/t_s, remained constant, showing no significant trend with relative density ($p > 0.05$), as shown in Fig. 4a. Additionally, it can be seen that the relative thickness was approximately 14%, indicating that the thickness of the pore walls was roughly an order of magnitude smaller than that of the struts. Fig. 4b also shows a comparison between the measured values for strut thickness and those calculated from the geometrical analysis of an open-cell tetrakaidecahedron material, which produced larger values in all cases.

Quantitative pore size measurements from Micro-CT confirmed the absence of any significant trend with relative density ($p > 0.05$), as shown in Fig. 5a. However, the measurements of percolation diameter showed a systematic decrease with increasing relative density, a trend which was found to be statistically significant ($p < 0.05$). This decrease in characteristic transport pathway diameter was also accompanied by an increase in measured *SSA*, as shown in Figure 5b. However, the increase in *SSA* was small compared with the difference between the measured results and those calculated for SSA_{open} [23], which appeared always much smaller.

Using the measured values of pore size and*SSA*, pore coverage fraction, γ, was calculated for each concentration, as shown in Fig. 6. The increase in γ with relative density was found to be statistically significant ($p < 0.05$). Overall, these results indicate that in addition to producing thicker pore walls, an increase in relative density produces a pore structure morphologically closer to that of a closed-cell model.

3.2. Hydration and swelling

The 3D Micro-CT images in Fig. 7 provide a representative view of the pore structures observed in the dry and hydrated states. All images shown indicate an isotropic pore structure for each condition, with very little change in pore size as concentration increased. It is also evident from these images that very little visible change in pore structure occurred on hydration. However, the scans from the hydrated scaffolds contain more noise, particularly for the smaller collagen concentrations.

Fig. 8 displays the effect of hydration in terms of bulk swelling of the scaffolds. Each trend is plotted as a function of hydrated relative density. It was observed that whereas the mass swelling ratio decreased with relative density, the volume swelling increased, with both trends found to be statistically significant ($p < 0.05$). To investigate this phenomenon further, the free water within the pore space was removed, allowing the relative contributions of free

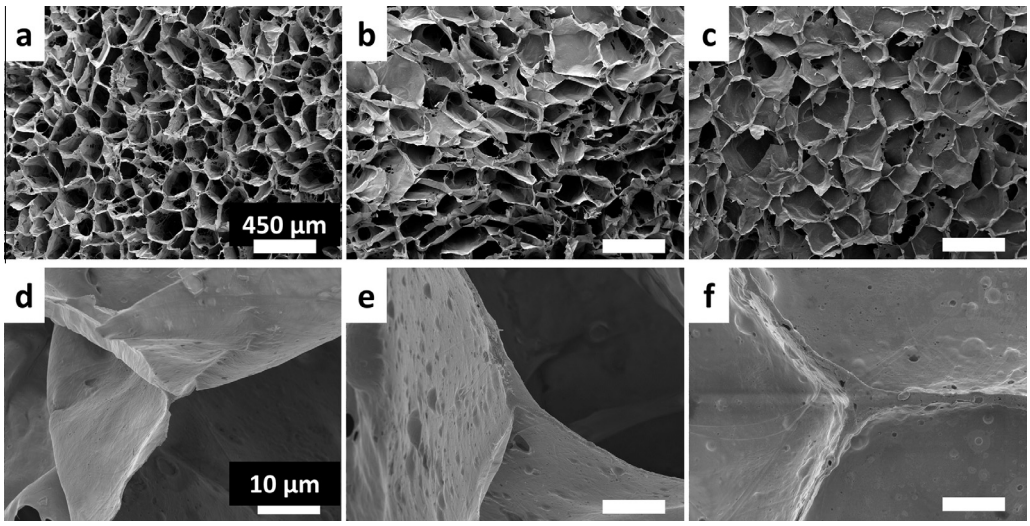

Fig. 3. Representative SEM micrographs of bulk collagen scaffolds (a–c), and triple points between pore walls (d–f) as a function of concentration in the precursor slurry: (a,d) 0.5%, (b,e) 1%, (c,f) 1.5%. While the bulk structure is qualitatively similar for all conditions, the size of the morphological features (pore strut and wall thicknesses) increases with collagen concentration.

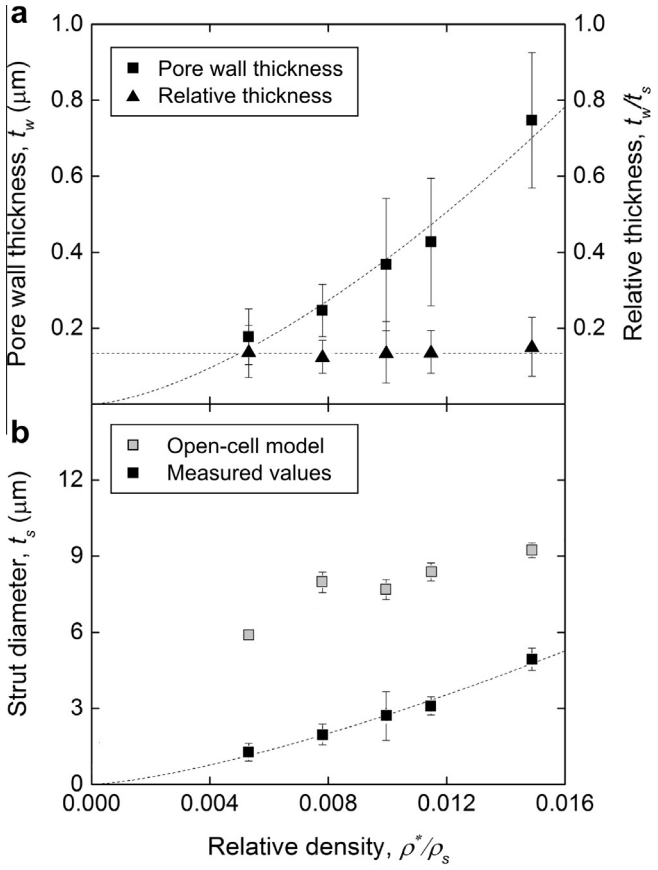

Fig. 4. (a) Pore wall thickness, t_w, and relative thickness to the diameter of pore struts, t_w/t_s. (b) Strut diameter, t_s, as measured and as predicted by the open-cell model [23]. The mean and standard deviation of 20 measurements are given. The dashed lines provide a guide to the eye to highlight the increase in morphological feature size with scaffold relative density.

water uptake and swelling of the pore walls to be measured. As shown in Fig. 9a, the amount of water bound to the collagen pore walls was constant when normalized over the scaffold dry mass, with no significant trend with relative density ($p > 0.05$). Additionally, Fig. 9b shows that the swelling of the free pore volume upon scaffold hydration was constant within the range of relative densities under investigation ($p > 0.05$), with a 20% increase in pore volume observed for all conditions.

These calculations of bulk swelling characteristics may be compared with the pore sizes measured from the hydrated scaffolds, as shown in Fig. 10. It is apparent that, as for the dry pore sizes discussed above, there was no trend in hydrated pore size with slurry concentration. Furthermore, the hydrated pore size measurements showed no significant difference to the dry measurements ($p > 0.05$), in comparison with the effects of measurement variability, indicated by the standard deviation. This level of variation is particularly apparent for the lower solid fractions, which correspond to the hydrated Micro-CT scans with greatest noise level, as is visible in the relevant images in Fig. 7.

3.3. Mechanical properties

Fig. 11 shows that the scaffold compressive modulus increased with relative density, in both the dry (viscoelastic) and hydrated (viscoelastic and poroelastic) states. For simplicity, only the poroelastic results are shown for the hydrated scaffolds, as the viscoelastic ones were found to follow the same trend. All such trends were found to be significant ($p < 0.05$) and very close to the quadratic relationship expected for open-cell materials [23], where deformation occurs by bending of the struts, with $n = 2.4 \pm 0.3$ ($R^2 = 0.96$) and $n = 2.0 \pm 0.2$ ($R^2 = 0.93$) for the dry and hydrated states respectively. Fig. 11 also shows linear ($n = 1$) and cubic ($n = 3$) relationships for comparison. These correspond to the behavior expected for a closed-cell material where deformation occurs by pore wall stretching and bending, respectively [30].

As shown in Fig. 12a, the Poisson's ratio of the hydrated materials also increased significantly with relative density ($p < 0.05$). The values shown are for the de-gassed samples only, and are all below the value expected for an incompressible fluid ($\upsilon = 0.5$), indicating the contribution of fluid flow. Although out of scope in the present study, it is worth mentioning that a similar investigation of non-degassed samples led to Poisson's ratios below zero at small relative densities, indicative of lateral collapse due to the presence of air pockets within the pore structure.

The viscoelastic ratio measurements shown in Fig. 12b were observed to be larger in the hydrated than in the dry state, as pre-

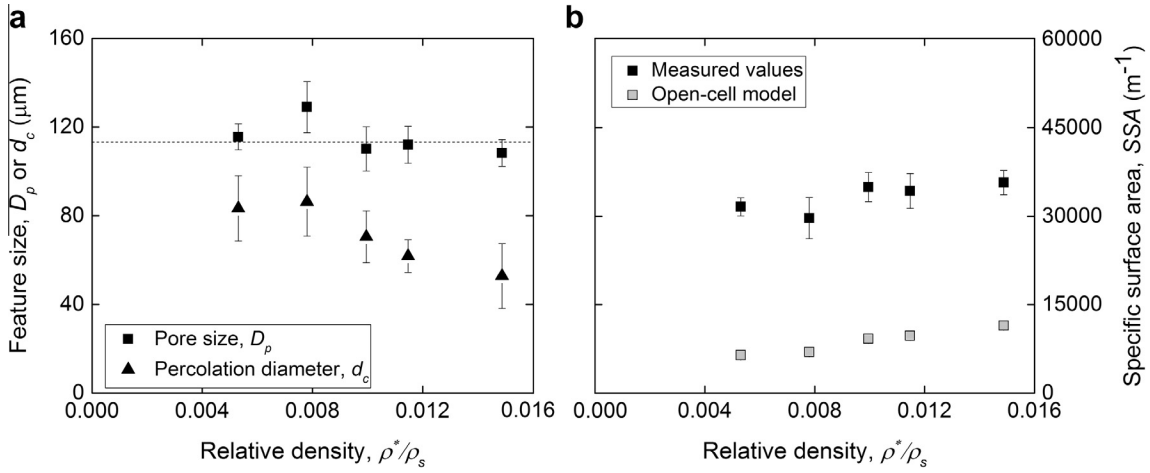

Fig. 5. (a) Pore size and percolation diameter, given as mean and standard deviation of the measurements from six regions per condition, and (b) specific surface area as a function of relative density, given as the mean and standard deviation of three measurements. While the pore size remains constant between conditions, the size of transport pathways in the materials become smaller with increasing solid concentration. In (b) the specific surface area expected for an open-cell material with the same pore size and concentration of collagen is also shown and observed to be much smaller than that measured due to the presence of pore walls.

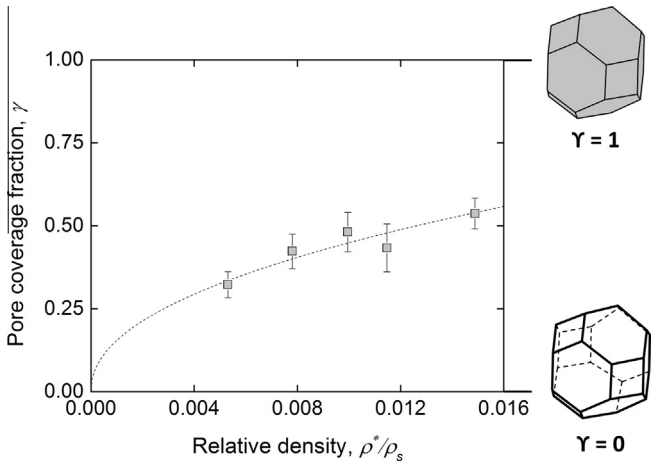

Fig. 6. Pore coverage fraction as a function of scaffold relative density. The dashed line provides a guide to the eye, highlighting the increasing pore closure with relative density.

viously reported [19]. In particular, it can be seen that whereas the viscoelastic ratio remained constant in the dry state ($p > 0.05$), it increased significantly with concentration in the hydrated state ($p < 0.05$), approaching a value characteristic of an elastic ($R = 1$), rather than viscoelastic ($R = 0$), response.

Fig. 13a shows that as relative density increased, the hydraulic permeability also decreased significantly ($p < 0.05$). In this case, the values measured for degassed and non-degassed samples were comparable ($p > 0.05$). In addition, satisfactory agreement can be seen between the values obtained from direct measurements and from poroelastic analysis. Fig. 13b shows that the fluid mobility within the scaffolds may be correlated to percolation diameter, increasing by approximately one order of magnitude with increasing size of the transport pathways.

4. Discussion

The results presented in this study provide new insights into the relationship between the structure of freeze-dried microporous scaffolds and their observed physical properties, which may ultimately affect their functionality as tissue engineering scaffolds. Since the relative density of porous materials is known to be a key determining factor in terms of both fluid content and scaffold mechanical properties [20,21], systematic changes in relative density were examined for their influence on morphology and behavior, by control of the collagen concentration in the precursor slurry. Morphologically, the pore size remained virtually unchanged with collagen concentration. Although changing solid concentration has been associated with pore size variation in previous studies, the reported trends differ from study to study [10,31]. The consensus in the literature is that the pore size of a freeze-dried collagen scaffold depends primarily on the chosen temperature profile [32], which was kept constant throughout this study.

Contrary to the pore size, measurements of percolation diameter indicated a decrease in the characteristic diameter of the pore transport pathways with solid concentration. Since this occurred at constant pore size, the likely explanation is that the scaffold structures at large solid concentrations approached that of a closed-cell model. This result is supported by the measurements of *SSA* and the calculation of the pore coverage fraction, which suggested that the fraction of pore walls increased with solid concentration. A larger surface area has previously been shown to improve the survival of cells seeded in the structure [12]. However, as the morphology of these scaffolds approaches a closed-cell nature, the accessibility of the scaffolds to cell invasion may become a crucial consideration: poor scaffold transport properties as characterized by small percolation diameters have previously been shown to inhibit fibroblast invasion [33].

Morphologically, all structural parameters were influenced by relative density: in addition to the increasing number of closed pore walls described above, the results in Figs. 3 and 4 show that the thicknesses of the pore walls and struts also increased as solid concentration increased. The ratio between the two, however, remained constant for all concentrations, with the strut diameter consistently an order of magnitude larger than the pore wall thickness. It is therefore expected that, in this case, the stress imposed on the scaffolds will be mainly carried by the struts [30]. This clarifies the observation that, despite the presence of pore walls within the scaffolds, the observed mechanical response showed a quadratic relationship between modulus and relative density: a response typical of open-cell foams [30]. This relationship was found to apply in both the dry and hydrated states, consistent with previous studies in which freeze-dried collagen scaffolds have been modeled as open-cell foams [21].

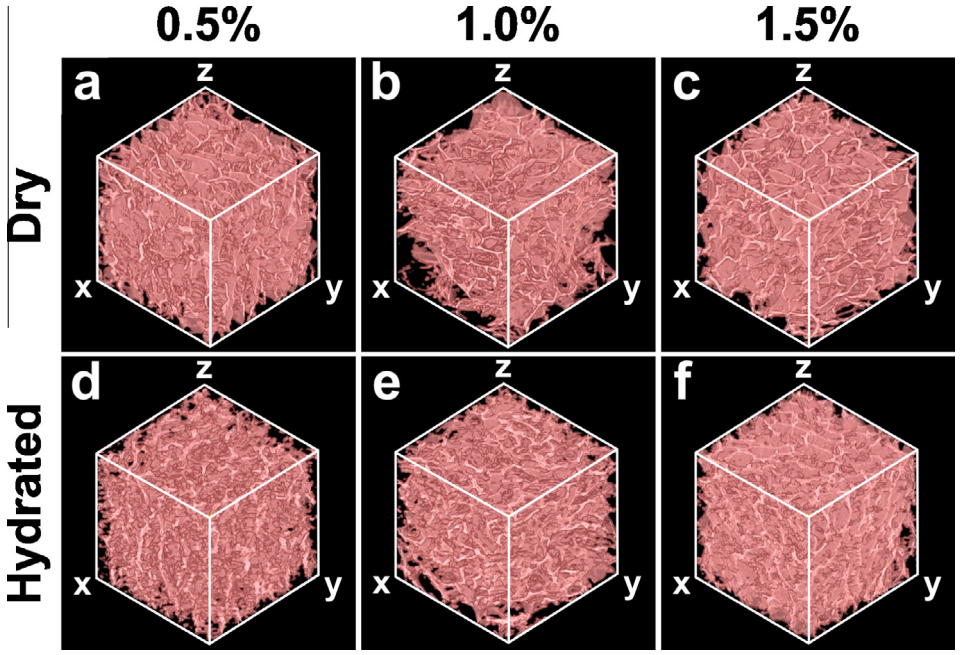

Fig. 7. Representative Micro-CT images of the pore structures in 3D, according to the collagen concentration in the precursor slurry, shown before (a–c) and after (d–f) hydration. Very little difference in pore structure is distinguishable from these images, on hydration or on variation of collagen concentration, although the noise level of the hydrated scans increases at low solid concentration. Each Micro-CT volume represents 1 mm^3.

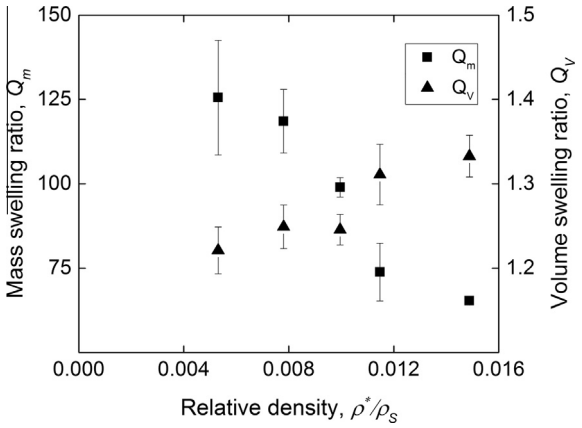

Fig. 8. Mass and volume swelling of the scaffolds after hydration, as a function of the scaffolds' dry relative density. These two measurement approaches produce opposite trends with relative density, with an increasing volume swelling but decreasing mass swelling ratio.

Unlike the modulus, the time-dependent response of the materials was affected by the presence of pore walls. In particular, the load relaxation in the hydrated state, as characterized by the viscoelastic ratio, was seen to decrease in magnitude as relative density, and therefore pore coverage fraction, increased (Fig. 12). It is likely that this behavior stemmed from fluid flow, since values of Poisson's ratio below 0.5, such as those shown in Fig. 12a, indicate fluid extrusion out of the scaffold. As water is retained in the structure, it may provide additional pressure that prevents the buckling of the structure over time. The increasing Poisson's ratio as relative density increases therefore suggests that fluid mobility was hindered at greater solid fractions, which correspond to the scaffolds with smaller percolation diameters and larger pore coverage fractions. The mechanical response also became progressively more elastic and less viscoelastic in nature, as a result of the small hydraulic permeability at large solid fractions shown in Fig. 13. The correlation shown in Fig. 13b indicates that this change in hydraulic permeability was strongly related to scaffold structure, with the increasing number of pore walls at large relative densities decreasing the availability of transport pathways for fluid flow.

The small hydraulic permeability at large relative densities has important implications for the ability of seeded cells to receive nutrients and eliminate waste. Although beyond the scope of this paper, it is interesting to note that the permeability results reported here are two orders of magnitude smaller than those previously reported for materials of similar structure [20]. However, it is recognized that comparison between permeability results obtained in different studies is currently extremely difficult, due to the variety of methods available for its measurement [34]. Nevertheless, the relatively slow flow rates used for direct permeability measurement in this study produced results consistent with those obtained by indentation, as has been observed in the past for hydrogels [35]. Most crucially, both methods show a clear relationship between permeability and scaffold structure, with fluid flow impeded by the structural arrangement at large relative densities.

Structural characterization in the dry state is often much more straightforward than in the hydrated state, leading to the common but necessary assumption that any morphological differences between the two states are minimal. Here it was shown, not only that the volume swelling experienced by the scaffolds is constant with relative density, but that the associated change in pore size is very small relative to the variability inherent in its measurement. This was confirmed both by direct measurements from Micro-CT, and also by calculation from measurements of bulk swelling, which indicated that the pore volume increased by a factor of 1.2 on hydration, for all conditions. This would be expected to correspond to a pore size change of $(1.2)^{\frac{1}{3}}$, i.e. roughly 6%. These results therefore validate the assumption that scaffold structure is largely constant on hydration, justifying the correlation between morphological properties in the dry state and the physical properties of hydrated scaffolds.

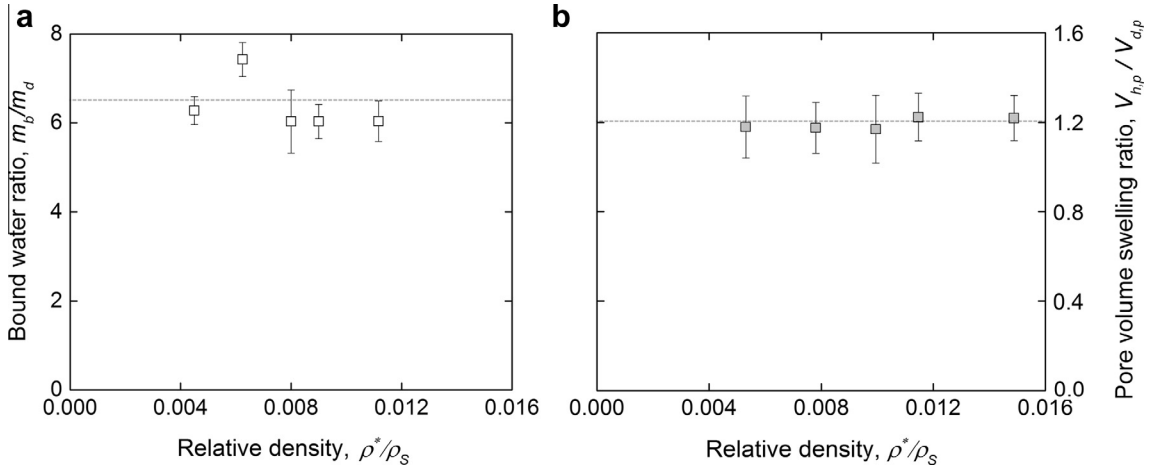

Fig. 9. (a) Bound water per dry mass of collagen in the scaffolds, and (b) free pore volume swelling, shown as a function of relative density. Both ratios are constant with scaffold relative density.

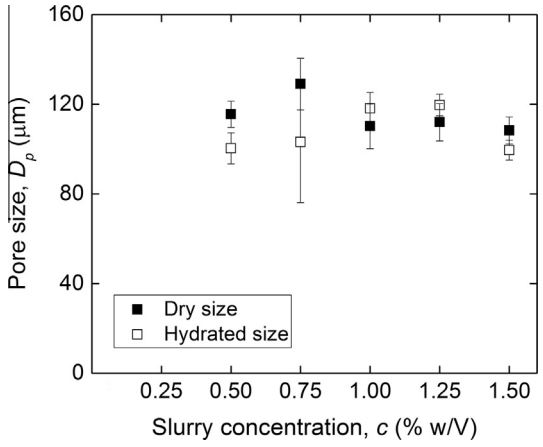

Fig. 10. Pore size measurements from Micro-CT scans of (a) dry scaffolds and (b) hydrated scaffolds. No change in pore size on hydration is detectable, due to its relatively small magnitude in comparison with measurement variability.

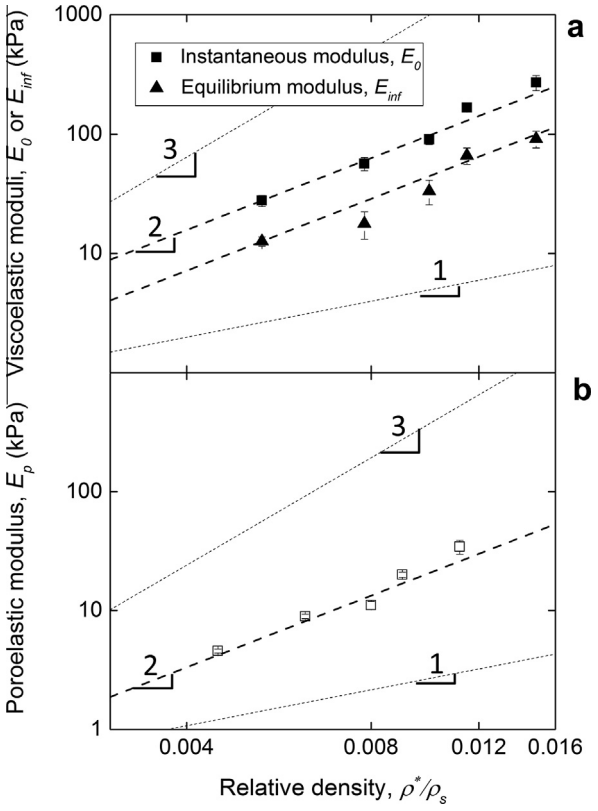

Fig. 11. Young's moduli of (a) dry and (b) hydrated scaffolds varying quadratically with relative density. The dashed lines provide a guide to the eye comparing a linear, quadratic and cubic dependency between modulus and relative density.

Conventional, nanoporous soft materials such as hydrogels present proportional mass to volume swellings, both inversely proportional to the amount of cross-linking [36]. However, the results in Fig. 8 clearly show that, in the case of microporous scaffolds made from cross-linked solids, the mass and volume swelling measurements produced opposite trends. As discussed above, the pore space available for free water does not change substantially with relative density, therefore any trend must be primarily due to the solid fraction. Since the mass of water bound to the collagen was constant when normalized to the dry mass, as shown by the bound water analysis in Fig. 9a, the swelling of the collagen itself was constant, irrespective of total concentration in the scaffold. The increase in volume swelling ratio can therefore be explained by the solid material swelling increasing in proportion to the solid concentration. It also provide further evidence that the nanoscale properties of the material making up the scaffolds remain the same, despite the varying properties of the materials at the bulk scale [19], and consistent with the constant amount of cross-linker added per solid mass. The cause of the decrease in mass swelling ratio, by far the most common parameter for describing hydration of these scaffolds [37,38], therefore appears to be entirely due to the normalization to scaffold dry mass involved in its calculation. The result, in this case, is to produce an intrinsic decrease in the mass swelling ratio as relative density increases. Swelling measurements in microporous scaffolds should therefore be interpreted with care, avoiding misleading definitions that do not describe their true physical behavior.

Overall, the results reported in this study indicate that the presence of pore walls is expected to influence the functionality of freeze-dried microporous materials as tissue engineering scaffolds. Although modeling these scaffolds as open-cell materials may be appropriate from a static mechanistic point of view, the pore closure fraction has implications for other physical properties. Extrapolation of the calculated trend for pore coverage fraction, Fig. 6, indicates that as the relative density approached zero, the

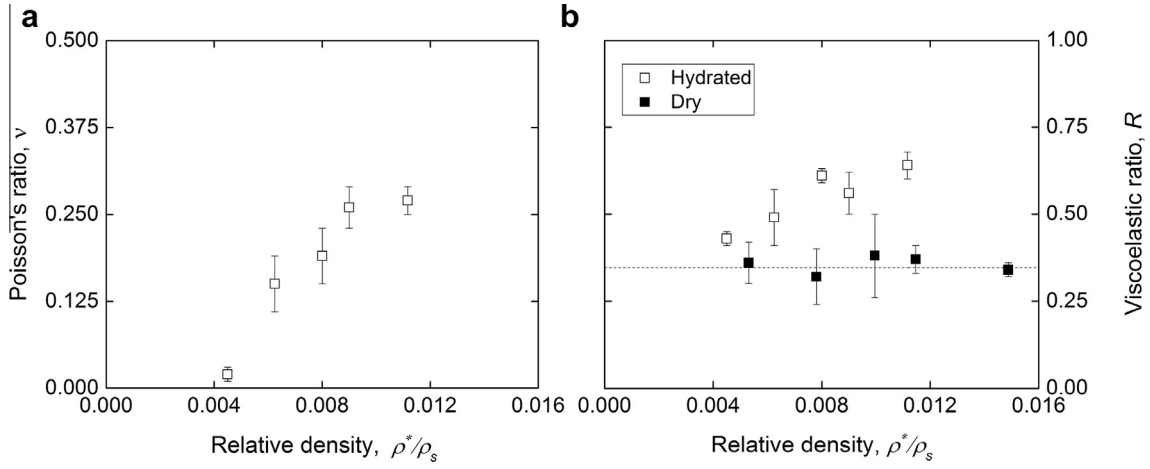

Fig. 12. Poisson's ratio (a) and viscoelastic ratio (b) as a function of scaffold relative density. The presence of fluid alters the time-dependent behavior of the materials and makes it density-dependent.

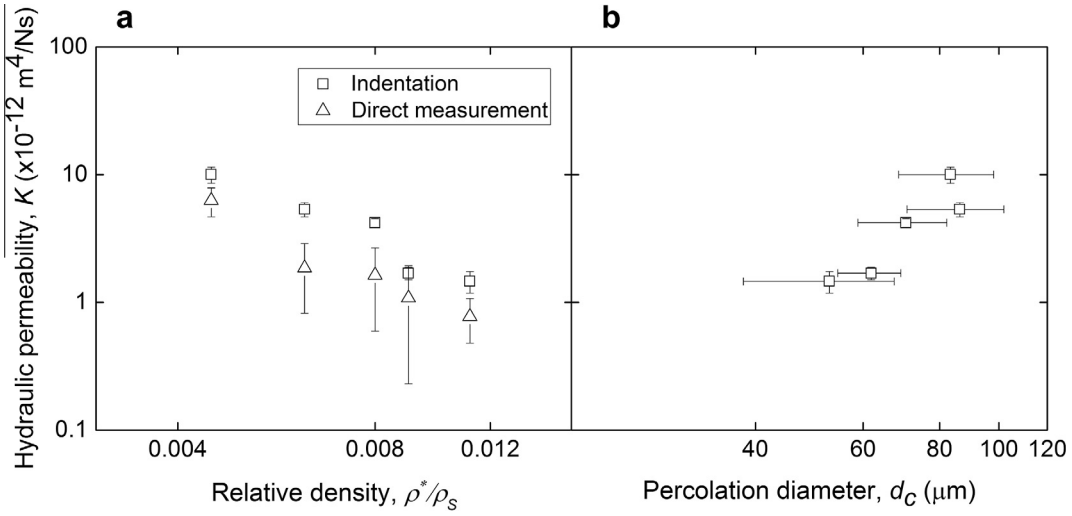

Fig. 13. Hydraulic permeability plotted as a function of (a) relative density, and (b) percolation diameter. The results for local testing by indentation in a poroelastic framework, and bulk testing on a custom-built rig are both shown in (a) for comparison.

structure tended towards the limit of an open-cell model. Percolation diameter also tended towards the pore size as relative density decreases. This suggests that the concerns about fluid mobility and cell accessibility become more relevant as relative density increases. However, since large relative densities may be preferable in terms of modulus and specific surface area, it may be that a balance is necessary in order to optimize the scaffold physical properties according to a chosen biological application.

5. Conclusions

Characterization of the morphology, hydration and mechanical properties of freeze-dried collagen scaffolds has provided new insights into the link between their structure and function. An increase in both pore wall closure and the thickness of pore walls and struts was observed on increasing relative density. These factors were found to determine the volume swelling on hydration, which increased in proportion to relative density. Pore size, however, remained relatively constant with relative density, and increased by only ~6% on hydration. Since this change is small relative to the inherent variability in its measurement, this validates the common assumption that morphological measurements in the dry state are representative of hydrated scaffolds. Crucially, although the dry and hydrated moduli of the bulk scaffolds were dependent on the pore struts alone, as expected of open-cell materials, the presence of pore walls dictated the fluid mobility within the scaffolds. This result has implications for the diffusion of nutrients and waste, the infiltration of cells, and also the time-dependent mechanical response. Therefore, modeling freeze-dried scaffolds solely as open-cell materials does not permit full optimization of scaffold functional design. Characterizing the deviation from this model is necessary in order to gain a full understanding of scaffold biophysical properties, including mechanical properties as well as accessibility to nutrient flow and cell invasion. This study provides a template that can be used to identify such deviation, ultimately optimizing scaffolds for specific tissue applications.

Acknowledgements

The authors are grateful to the EPSRC CDT in Nanoscience and Nanotechnology (NanoDTC), University of Cambridge, ERC

Advanced Grant No. 320598 3D-E, Geistlich Pharma AG and the EPSRC who supported this work through the Doctoral Training Account and the EP/G037221/1 grant. Supporting research data as required by EPSRC research policy may be accessed at https://www.repository.cam.ac.uk/handle/1810/253598.

Appendix A

In the dry state the mass of a scaffolds is m_d and its volume, V_d, is the sum of the volume occupied by collagen, $V_{S,d}$, and the free pore space, $V_{p,d}$. As the scaffold is hydrated, the mass is increased by that of the water imbibed in the scaffold, the sum of free and bound water, $m_f + m_b$. Similarly, the volume is the sum of the volume of hydrated collagen, $V_{S,h}$, and that of the free water-filled pore space, $V_{p,h}$. The volume swelling ratio is then:

$$Q_V = \frac{V_{S,h} + V_{p,h}}{V_{S,d} + V_{p,d}} \tag{9}$$

and the pore volume swelling ratio is:

$$\frac{V_{p,h}}{V_{p,d}} = \frac{Q_V\left(V_{S,d} + V_{p,d}\right) - V_{S,h}}{V_{p,d}} \tag{10}$$

The volumes taken into consideration can be further expressed as a function of measured or known quantities. Firstly, the dry volume of collagen is:

$$V_{S,d} = \frac{m_d}{\rho_S} \tag{11}$$

while the hydrated volume of collagen $V_{S,h}$ can be thought of as the sum of $V_{S,d}$ and the bound water volume, $\frac{m_b}{\rho_w}$, assuming the water bound to collagen has the same density ρ_w as that of free water. Secondly, the pore volume in the dry state is equal to the difference between the bulk dry volume and the volume of dry collagen:

$$V_{p,d} = V_d - V_{S,d} = \frac{m_d}{\rho^*} - \frac{m_d}{\rho_S} \tag{12}$$

Or, expressed in terms of the relative density of the scaffolds:

$$V_{p,d} = \frac{m_d}{\rho_S}\frac{\rho_S}{\rho^*} - \frac{m_d}{\rho_S} = V_{S,d}\left(\frac{\rho_S}{\rho^*} - 1\right) \tag{13}$$

so that substitution then gives:

$$\frac{V_{p,h}}{V_{p,d}} = \frac{Q_V\left[V_{S,d} + V_{S,d}\left(\frac{\rho_S}{\rho^*} - 1\right)\right] - V_{S,d} - \frac{m_b}{\rho_w}}{V_{S,d}\left(\frac{\rho_S}{\rho^*} - 1\right)} \tag{14}$$

or, dividing by $V_{S,d}$:

$$\frac{V_{p,h}}{V_{p,d}} = \frac{Q_V\frac{\rho_S}{\rho^*} - 1 - \frac{m_b}{m_d}\frac{\rho_S}{\rho_w}}{\frac{\rho_S}{\rho^*} - 1} \tag{15}$$

References

[1] J. Hunsberger, O. Harrysson, R. Shirwaiker, B. Starly, R. Wysk, P. Cohen, J. Allickson, J. Yoo, A. Atala, Manufacturing road map for tissue engineering and regenerative medicine technologies, Stem Cells Transl. Med. 4 (2015) 130–135.

[2] M.J. Webber, O.F. Khan, S.A. Sydlik, B.C. Tang, R. Langer, A perspective on the clinical translation of scaffolds for tissue engineering, Annals of biomedical engineering 43 (3) (2015) 641–656.

[3] I.V. Yannas, D.S. Tzeranis, B.A. Harley, P.T.C. So, Biologically active collagen-based scaffolds: advances in processing and characterization, Philos. Trans. Ser. A Math. Phys. Eng. Sci. 368 (1917) (2010) 2123–2139.

[4] K.M. Pawelec, S.M. Best, R.E. Cameron, R.J. Wardale, Scaffold architecture and fibrin gels promote meniscal cell proliferation, APL Mater. 3 (014901) (2015).

[5] I.V. Yannas, Tissue regeneration by use of collagen-glycosaminoglycan copolymers, Clin. Mater. 9 (1992) 179–187.

[6] U. Cheema, M. Ananta, V. Mudera, Collagen: applications of a natural polymer in regenerative medicine, Regenerative Medicine and Tissue Engineering – Cells and Biomaterials, InTech – Open Access Publisher, 51000 Rijeka, Croatia, 2011, pp. 287–300.

[7] D.N. Tatakis, A. Promsudthi, U.M.E. Wikesjö, Devices for periodontal regeneration, Periodontol 2000 19 (1) (1999) 59–73.

[8] C.N. Grover, J.H. Gwynne, N. Pugh, S. Hamaia, R.W. Farndale, S.M. Best, R.E. Cameron, Crosslinking and composition influence the surface properties, mechanical stiffness and cell reactivity of collagen-based films, Acta Biomater. 8 (8) (2012) 3080–3090.

[9] K.M. Pawelec, A. Husmann, S.M. Best, R.E. Cameron, Ice-templated structures for biomedical tissue repair: from physics to final scaffolds, Appl. Phys. Rev. 1 (2) (2014) 21301.

[10] K.M. Pawelec, A. Husmann, S.M. Best, R.E. Cameron, A design protocol for tailoring ice-templated scaffold structure, J. R. Soc. Interface 11 (92) (2014) 20130958.

[11] K.M. Pawelec, A. Husmann, S.M. Best, R.E. Cameron, Understanding anisotropy and architecture in ice-templated biopolymer scaffolds, Mater. Sci. Eng.: C 37 (2014) 141–147.

[12] F.J. O'Brien, B.A. Harley, I.V. Yannas, L.J. Gibson, The effect of pore size on cell adhesion in collagen-GAG scaffolds, Biomaterials 26 (4) (2005) 433–441, http://dx.doi.org/10.1016/j.biomaterials.2004.02.052.

[13] H.W. Kang, Y. Tabata, Y. Ikada, Fabrication of porous gelatin scaffolds for tissue engineering, Biomaterials 20 (14) (1999) 1339–1344. URL <http://www.ncbi.nlm.nih.gov/pubmed/10403052>.

[14] H.W. Kim, H.E. Kim, V. Salih, Stimulation of osteoblast responses to biomimetic nanocomposites of gelatin-hydroxyapatite for tissue engineering scaffolds, Biomaterials 26 (25) (2005) 5221–5230, http://dx.doi.org/10.1016/j.biomaterials.2005.01.047.

[15] N. Sultana, M. Wang, PHBV/PLLA-based composite scaffolds fabricated using an emulsion freezing/freeze-drying technique for bone tissue engineering: surface modification and in vitro biological evaluation, Biofabrication 4 (1) (2012) 015003, http://dx.doi.org/10.1088/1758-5082/4/1/015003. URL <http://www.ncbi.nlm.nih.gov/pubmed/22258057>.

[16] V. Maquet, S. Blacher, R. Pirard, J.-P. Pirard, M.N. Vyakarnam, R. Jérôme, Preparation of macroporous biodegradable poly(L-lactide-co-epsilon-caprolactone) foams and characterization by mercury intrusion porosimetry, image analysis, and impedance spectroscopy, J. Biomed. Mater. Res. Part A 66 (2003) 199–213, http://dx.doi.org/10.1002/jbm.a.10523.

[17] Z. Li, H.R. Ramay, K.D. Hauch, D. Xiao, M. Zhang, Chitosan-alginate hybrid scaffolds for bone tissue engineering, Biomaterials 26 (18) (2005) 3919–3928, http://dx.doi.org/10.1016/j.biomaterials.2004.09.062.

[18] J.C. Ashworth, M. Mehr, P.G. Buxton, S.M. Best, R.E. Cameron, Parameterising the transport pathways for cell invasion in complex scaffold architectures, Tissue Eng.: Part C. (2015).

[19] G.S. Offeddu, J.C. Ashworth, R.E. Cameron, M.L. Oyen, Multi-scale mechanical response of freeze-dried collagen scaffolds for tissue engineering applications, J. Mech. Behav. Biomed. Mater. 42 (2015) 19–25.

[20] F.J. O'Brien, B.A. Harley, M.A. Waller, I.V. Yannas, L.J. Gibson, P.J. Prendergast, The effect of pore size on permeability and cell attachment in collagen scaffolds for tissue engineering, Technol. Health Care 15 (1) (2007) 3–17.

[21] B.A. Harley, J.H. Leung, E.C.C.M. Silva, L.J. Gibson, Mechanical characterization of collagen-glycosaminoglycan scaffolds, Acta Biomater. 3 (4) (2007) 463–474.

[22] Y.-G. Ko, N. Kawazoe, T. Tateishi, Preparation of novel collagen sponges using an ice particulate template, J. Bioact. Compatible Polym. 25 (4) (2010) 360–373.

[23] L.J. Gibson, M.F. Ashby, Cellular Solids: Structure and Properties, Cambridge University Press, 1999.

[24] H.M. Princen, P. Levinson, The surface area of Kelvin's minimal tetrakaidecahedron: the ideal foam cell (?), J. Colloid Interface Sci. 120 (1) (1987) 172–175.

[25] J. Zhu, R.E. Marchant, Design properties of hydrogel tissue-engineering scaffolds, Expert Rev. Med. Devices 8 (5) (2011) 607–626.

[26] M. Galli, E. Fornasiere, J. Cugnoni, M.L. Oyen, Poroviscoelastic characterization of particle-reinforced gelatin gels using indentation and homogenization, J. Mech. Behav. Biomed. Mater. 4 (4) (2011) 610–617.

[27] M.L. Oyen, Analytical techniques for indentation of viscoelastic materials, Phil. Mag. 86 (33–35) (2006) 5625–5641.

[28] M.L. Oyen, T.A.V. Shean, D.G.T. Strange, M. Galli, Size effects in indentation of hydrated biological tissues, J. Mater. Res. 27 (01) (2011) 245–255.

[29] J.A. Searles, J.F. Carpenter, T.W. Randolph, The ice nucleation temperature determines the primary drying rate of lyophilization for samples frozen on a temperature-controlled shelf, J. Pharm. Sci. 90 (7) (2001) 860–871.

[30] A. Roberts, E. Garboczi, Elastic moduli of model random three-dimensional closed-cell cellular solids (2000) 13arXiv:0009004.

[31] C.M. Tierney, M.G. Haugh, J. Liedl, F. Mulcahy, B. Hayes, F.J. O'Brien, The effects of collagen concentration and crosslink density on the biological, structural and mechanical properties of collagen-GAG scaffolds for bone tissue engineering, J. Mech. Behav. Biomed. Mater. 2 (2) (2009) 202–209.

[32] F.J. O'Brien, B.A. Harley, I.V. Yannas, L. Gibson, Influence of freezing rate on pore structure in freeze-dried collagen-GAG scaffolds, Biomaterials 25 (6) (2004) 1077–1086, http://dx.doi.org/10.1016/S0142-9612(03)00630-6.

[33] J.C. Ashworth, M. Mehr, P.G. Buxton, S.M. Best, R.E. Cameron, Cell invasion in collagen scaffold architectures characterized by percolation theory, Adv. Healthcare Mater. 4 (9) (2015) 1317–1321.

[34] F. Pennella, G. Cerino, D. Massai, D. Gallo, G. Falvo D'Urso Labate, A. Schiavi, M. A. Deriu, A. Audenino, U. Morbiducci, A survey of methods for the evaluation of tissue engineering scaffold permeability, Ann. Biomed. Eng. 41 (10) (2013) 2027–2041.
[35] D.G.T. Strange, M.L. Oyen, Composite hydrogels for nucleus pulposus tissue engineering, J. Mech. Behav. Biomed. Mater. 11 (2012) 16–26.
[36] L. Treloar, The Physics of Rubber Elasticity, Oxford University Press, 1975.
[37] L. Ma, C. Gao, Z. Mao, J. Zhou, J. Shen, X. Hu, C. Han, Collagen/chitosan porous scaffolds with improved biostability for skin tissue engineering, Biomaterials 24 (26) (2003) 4833–4841.
[38] S.-N. Park, J.-C. Park, H.O. Kim, M.J. Song, H. Suh, Characterization of porous collagen/hyaluronic acid scaffold modified by 1-ethyl-3-(3-dimethylaminopropyl)carbodiimide cross-linking, Biomaterials 23 (4) (2002) 1205–1212.